Discrete Element Method Simulations for Complex Granular Flows

Yu Guo and Jennifer Sinclair Curtis

Department of Chemical Engineering, University of Florida, Gainesville, Florida 32611-6005; email: guoyu03@gmail.com, jcurtis@che.ufl.edu

Annu. Rev. Fluid Mech. 2015. 47:21–46

First published online as a Review in Advance on June 23, 2014

The *Annual Review of Fluid Mechanics* is online at fluid.annualreviews.org

This article's doi: 10.1146/annurev-fluid-010814-014644

Keywords

particle shape, particle cohesion, particle breakage, particle flexibility

Abstract

This review article focuses on the modeling of complex granular flows employing the discrete element method (DEM) approach. The specific topic discussed is the application of DEM models for the study of the flow behavior of nonspherical, flexible, or cohesive particles, including particle breakage. The major sources of particle cohesion—liquid induced, electrostatics, van der Waals forces—and their implementation into DEM simulations are covered. These aspects of particle flow are of great importance in practical applications and hence are the significant foci of research at the forefront of current DEM modeling efforts. For example, DEM simulations of nonspherical grains can provide particle stress information needed to develop constitutive models for continuum-based simulations of large-scale industrial processes.

1. INTRODUCTION

Processes involving particulate or granular flows are prevalent throughout the pharmaceutical, chemical, energy, food handling, mineral processing, powder metallurgy, and mining industries. In addition, numerous phenomena found in nature involve such material flows. To understand the complex, macroscopic behavior of granular materials and then reliably design, scale up, control, or optimize their flow, researchers need details about the interactions between individual particles (i.e., the microscopic mechanisms that control the macroscopic behavior). One simulation technique, the discrete element method (DEM), has become widely implemented over the past three decades for the study of granular flows since it was introduced by Cundall & Strack (1979).

In the DEM technique, the motion of each individual particle is governed by Newton's second law of motion,

$$m_i \frac{\mathrm{d}\mathbf{v}_i}{\mathrm{d}t} = \mathbf{F}_i^C + m_i\mathbf{g} + \mathbf{F}_i^{\mathrm{fp}}$$

and

$$\mathbf{I}_i \cdot \frac{\mathrm{d}\boldsymbol{\omega}_i}{\mathrm{d}t} - (\mathbf{I}_i \cdot \boldsymbol{\omega}_i) \times \boldsymbol{\omega}_i = \mathbf{T}_i,$$

where $\mathbf{v}_i$ and $\boldsymbol{\omega}_i$ are the translational and angular velocities, respectively, of the particle i of mass m_i and moment of inertia tensor $\mathbf{I}_i$. The translational motion of the particle is normally driven by the interparticle contact force $\mathbf{F}_i^C$, gravitational force $m_i\mathbf{g}$, and the fluid-particle interaction force $\mathbf{F}_i^{\mathrm{fp}}$ if fluid media exist in the particulate system. Also, the particle rotation may be induced by the torque $\mathbf{T}_i$ arising from particle-particle contact and fluid-particle interaction. The evolution of some particle-scale quantities, such as the particle velocity, position, orientation, and contact force, can be obtained by the time integration of the equations of motion, which is implemented in the DEM code based on a computational sequence, as illustrated in **Figure 1**. Based on knowledge of these particle-scale quantities, one can predict bulk behaviors of interest—the particle packing density, angle of repose, mass flow or discharge rate, agglomerate size, blend uniformity, and particle phase stress. To date, DEM simulations have been successfully applied to a wide gamut of applications and have successfully reproduced well-known particle flow features observed in practice.

Owing to the widespread research developments in this field and the application of the DEM as a core tool for their studies, several excellent articles have been published regarding granular flows and the DEM. Forterre & Pouliquen (2008), Campbell (1990, 2006), Jenkins (2006), and Goldhirsch (2003) reviewed the flow regimes, microstructure, and development of constitutive relations for granular media based on theoretical analyses, DEM simulations, and experimental studies. Li et al. (2011), Luding (2008), Zhu et al. (2007, 2008), and Kruggel-Emden et al. (2007) have provided recent reviews of the DEM. These articles focus on the governing equations, normal and tangential (frictional) contact force models, and several applications of the DEM (e.g., particle packing, flows in hoppers, mixers, rotating drums, and ball mills). Li et al. (2011) and Zhu et al. (2007, 2008) also discussed the simulation of discrete particle flow coupled with fluid (gas and/or liquid) via the computational fluid dynamics–DEM approach and emphasized fluid-particle interaction forces. The basic mechanics of DEM, including the choice of contact parameters and the implementation of the numerical scheme, are outlined by Mishra (2003), Williams & O'Connor (1999), Thornton (1999), Barker (1994), and Walton (1994).

Therefore, this article outlines some of the most recent and significant topics in DEM development and application that have not been reviewed more comprehensively before. Hence, it is not intended to provide or represent an exhaustive survey of the subject. The topics discussed include DEM models for the study of the complex flow behavior associated with nonspherical, flexible, or

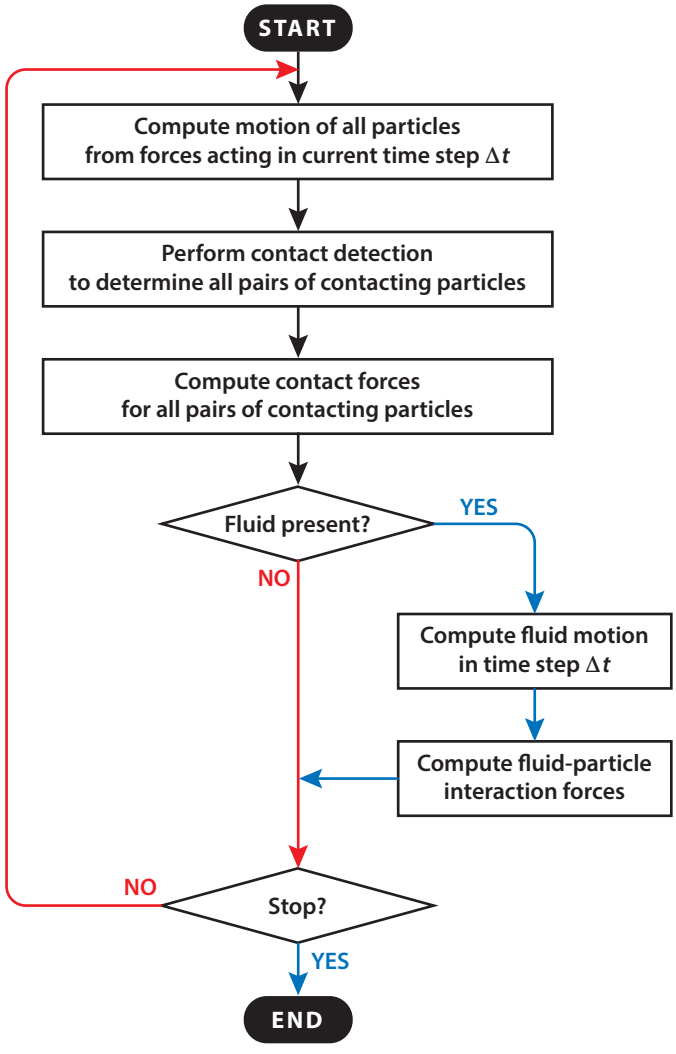

Figure 1

Flow chart of computational sequence in a typical discrete element method code.

cohesive particles. Major sources of particle cohesion—liquid induced, electrostatics, and van der Waals forces—and their implementation into DEM simulations are covered. Because of computational limitations, early DEM simulations considered only interactions of circular disks in two dimensions or spheres in three dimensions owing to the well-established contact force model, the simplicity of contact detection, and the extremely limited number of particles that could be simulated. However, current developments in the DEM focus on the effect of particle shape using ellipsoids, cylinders or spherocylinders, superquadrics, polyhedra, or glued-sphere clusters involving linking and overlapping spheres. Descriptions for nonspherical particles have also been recently extended to model flexible grains and particle breakage. All these aspects—particle cohesion, sphericity, flexibility, and breakage—are of great importance in practical/industrial applications involving granular flows, and these are the subjects emphasized here.

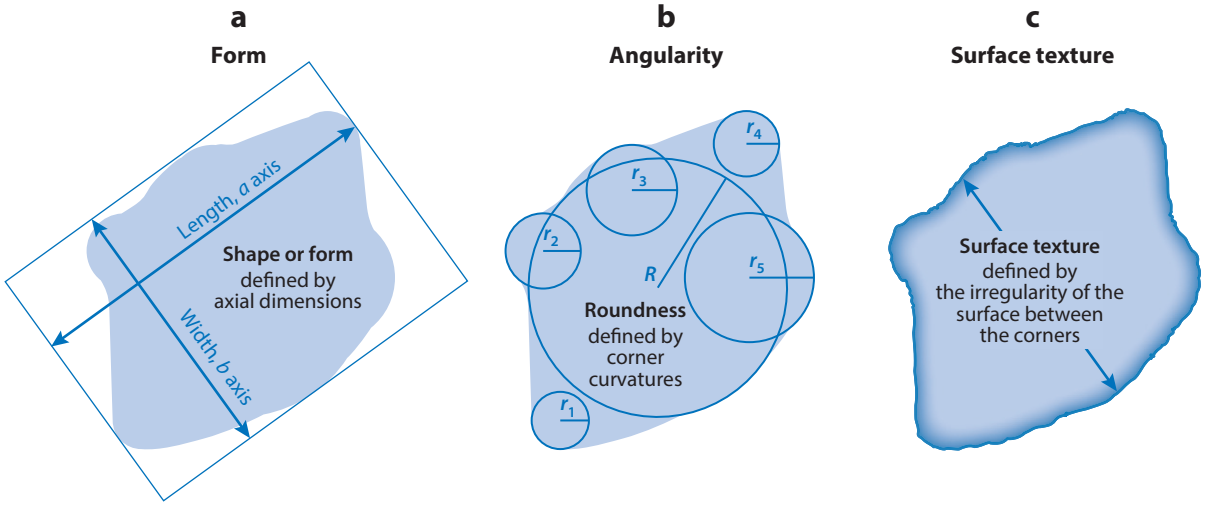

Figure 2

Schematic illustration of three shape descriptors: (*a*) form, (*b*) angularity, and (*c*) surface texture. Figure adapted with permission from Tafesse et al. (2012), © 2012 the authors. Journal compilation © 2012 International Association of Sedimentologists.

2. EFFECT OF PARTICLE SHAPE

As particle shape is recognized as one of most important parameters influencing the behavior of granular materials, the DEM has been advanced for the modeling of nonspherical particles, including ellipses (Cleary 2008), polygons (Peña et al. 2007), spheroids (Campbell 2011), cylinders (Guo et al. 2012, 2013c; Kodam et al. 2010), polyhedra (Azéma et al. 2013), and the irregularly shaped particles represented by sphere clusters (Katagiri et al. 2010). To quantify the particle shape, researchers (Krumbein & Pettijohn 1938; Tafesse et al. 2012) have proposed three major morphological descriptors: form, angularity, and surface texture (**Figure 2**). Form is used to describe the dimensional difference of a particle in the principal axes and is usually quantified in terms of sphericity. Sphericity is the ratio of the surface area of the equivalent volume sphere (the same volume as the particle) to the surface area of the particle. In particular, the elongation of a spheroid is quantified using the aspect ratio, defined as the length ratio of the major axis to the minor axis. Angularity is a descriptor of the variations in corners and faces. Several definitions of angularity have been proposed and compared (Tafesse et al. 2012). A typical angularity index is defined as follows (Lees 1964):

$$\mathrm{AI} = \sum_{i=1}^{n} (180 - \alpha_i)\frac{x_i}{r},$$

where α_i is the angle measured between planes bounding corner i, x_i is the distance from the center of the maximum inscribed circle to the tip of corner i, r is the radius of the maximum inscribed circle, and n is the number of corners. For a three-dimensional particle, one can estimate the degree of angularity by the average value of the angularity index of the projected images in three perpendicular directions. Surface texture describes the roughness of the surface of a particle, reflecting the small-scale details on the particle surface.

DEM modeling provides the microstructural information of a bulk granular material, facilitating the understanding of the effect of particle shape on granular texture and interparticle contacts. It has been found that the packing density initially increases and then decreases with the increase

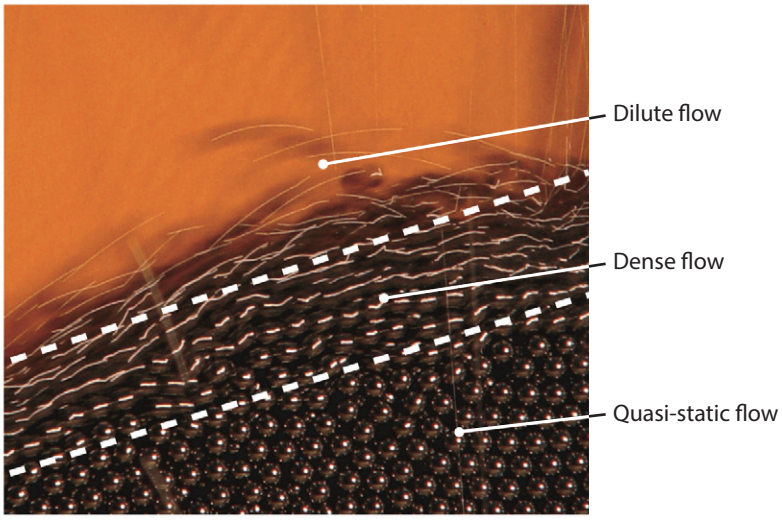

Figure 3

An illustration of dilute flow, dense flow, and quasi-static flow in the process of pouring steel beads on a pile. Figure adapted with permission from Forterre & Pouliquen (2008) from the *Annual Review of Fluid Mechanics*, Volume 40, by Annual Reviews (**http://www.annualreviews.org**).

in particle elongation (Azéma & Radjaï 2010, 2012; Guises et al. 2009; Wouterse et al. 2007), angularity (Azéma et al. 2013), or platyness (Boton et al. 2013, Wouterse et al. 2007). The slight shape deviation from a sphere can improve the particle tessellating capability and increase the packing density. However, larger void space may be created owing to the formation of bridging and arching structures as the particles become more elongated, more angular, or flatter.

Granular flows can be classified into three regimes: dilute flow, dense flow, and quasi-static flow (**Figure 3**). In dilute flow, binary and instantaneous collisions are dominant, and the stress is proportional to the square of the shear rate. Dilute flow is also known as gas-like flow or inertial flow. In dense flow, multiple and enduring contacts are dominant, and the stress is proportional to the shear rate. Dense flow is also recognized as liquid-like flow or elastic-inertial flow. In quasi-static flow, a densely packed bed of particles is sheared at a low rate, and the stress is independent of the shear rate. Quasi-static flow behavior is also recognized as solid-like behavior or elastic-quasi-static behavior.

DEM simulations have been performed to study the effect of particle shape on all three flow regimes. Guo et al. (2013c) simulated three-dimensional periodic shear flows of elongated rods and flat disks at various solid volume fractions and discussed the effects of particle elongation and flatness. **Figure 4** shows the normalized shear stress as a function of the solid volume fraction for cylindrical particles of different aspect ratios. The particle phase stress tensor $\boldsymbol{\sigma}$ can be expressed as the sum of a kinetic component and a collisional component. The kinetic component, which arises from the momentum transfer by particles as they move through the bulk material, is given by

$$\boldsymbol{\sigma}_{\text{kin}} = \rho\nu \langle \mathbf{VV} \rangle ,$$

where ρ and ν represent the particle density and solid volume fraction, respectively. The brackets represent an average over time and volume, and $\mathbf{V} = \mathbf{v}_i - \langle \mathbf{v} \rangle$ is the fluctuating velocity of particle i. The average velocity $\langle \mathbf{v} \rangle$ is the local steady-state, shear velocity. The collisional component, which

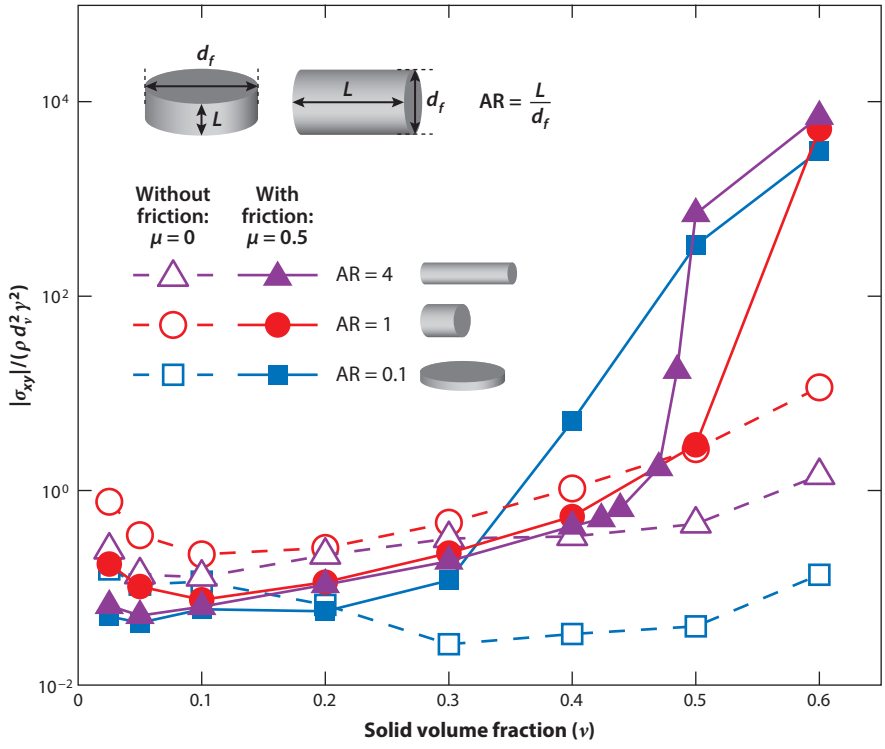

Figure 4

Normalized shear stress as a function of solid volume fraction for cylindrical particles of different aspect ratios (ARs) with and without friction. The coefficient of restitution e is 0.95, and Young's modulus E is 8.7×10^9 Pa. Figure reproduced with permission from Guo et al. (2012, 2013c).

arises from the momentum transfer from one point to another in the material by interparticle collisions, is written as

$$\boldsymbol{\sigma}_{\text{col}} = \langle \mathbf{F}_i^j \mathbf{l}_{ij} \rangle,$$

where $\mathbf{F}_i^j$ is the contact force exerted on particle i by particle j, and $\mathbf{l}_{ij}$ represents the vector from the mass center of particle i to the mass center of particle j. In the simulations, the stress measurements were made by calculating the kinetic and collisional components and summing them. In **Figure 4**, the magnitude of the shear stress component $|\sigma_{xy}|$ is normalized by $\rho d_v^2 \gamma^2$, where d_v is the equivalent volume diameter of the particle and γ is the shear rate. The aspect ratio of a particle is defined as the ratio of cylinder length L to the diameter of circular end face d_f (i.e., AR $= L/d_f$). Rods and disks correspond to aspect ratios greater than 1 and less than 1, respectively. It is evident that particle shape has an impact on granular stresses with and without friction.

2.1. Dilute Flow

For dilute flow, the main contributor to its stress is the kinetic stress, which is proportional to the particle fluctuating velocity squared. According to recent DEM simulation work (Guo et al. 2012), the elongation of particles leads to an increase in the effective projected area of the particles on the plane perpendicular to the flow direction; therefore, the particle collision frequency increases.

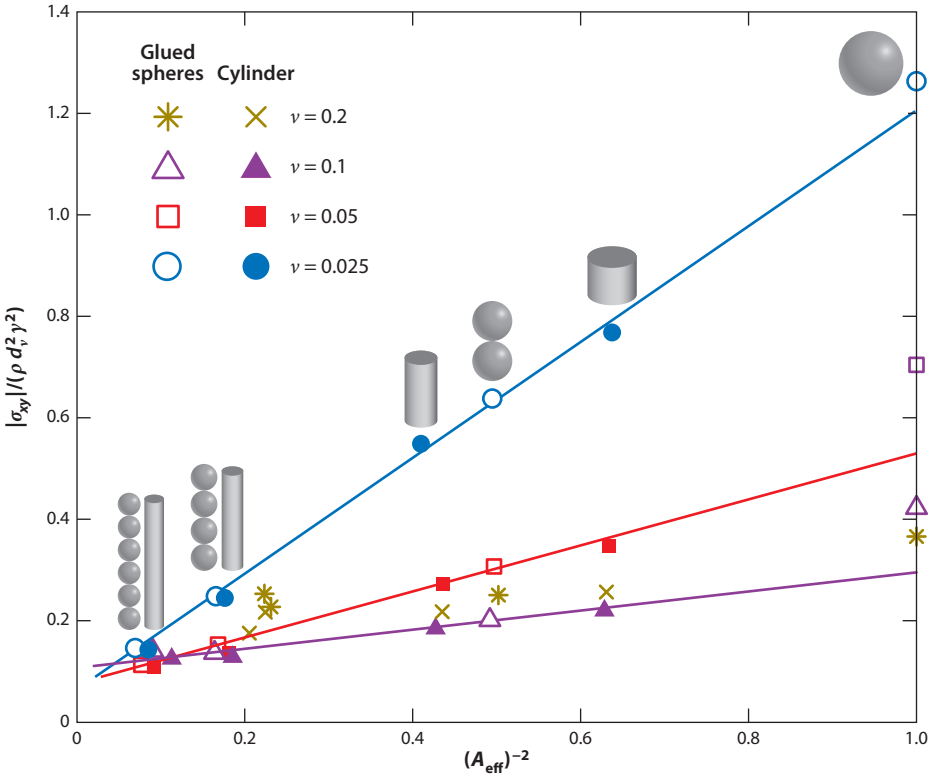

Figure 5

Normalized shear stresses as a function of the negative square of the normalized particle projected area for dilute flow at different low solid volume fractions. Figure adapted with permission from Guo et al. (2012).

Actually, the effective projected area can also be increased by making the particles flatter. Because the particle fluctuating velocity is inversely proportional to the particle collision frequency, the stress in dilute flow is reduced as the particles are elongated. As shown in **Figure 5**, the stress and the particle projected area at lower solid volume fractions (e.g., $\leq$0.1) follow a relationship for all particle aspect ratios,

$$\frac{\sigma_{xy}}{\rho d_v^2 \gamma^2} \propto \frac{1}{(A_{\text{eff}})^2},$$

where A_{eff} is the normalized effective projected area:

$$A_{\text{eff}} = \frac{S_{\text{eff}}}{S_{\text{sph}}},$$

where S_{eff} is the effective projected area of a particle on the plane perpendicular to the flow direction, and S_{sph} is the effective projected area of the sphere of the same volume to the particle (Guo et al. 2012). Scaling relationships of this kind are convenient for the development of constitutive relations for stress, which can subsequently be employed in continuum-based simulations for particle flow. However, the linear relationship between the stress and $(A_{\text{eff}})^{-2}$ is violated as the solid volume fraction reaches 0.2, when the collisional stress contributes a significant portion to the total granular stress.

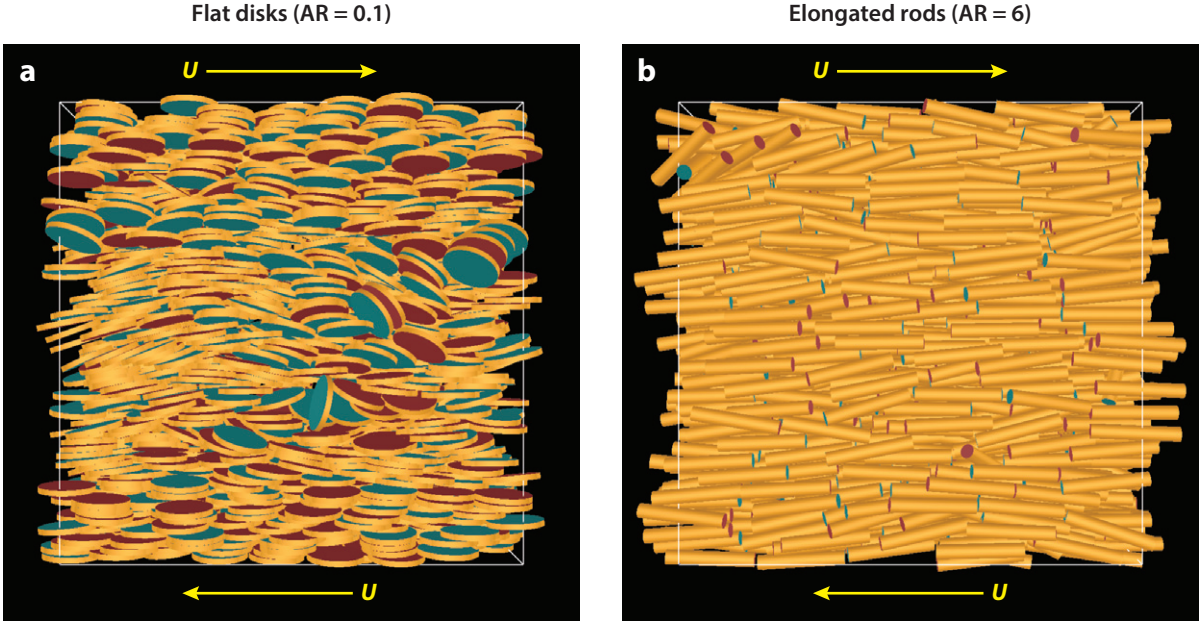

Figure 6

Alignment of (*a*) disks and (*b*) elongated rods at a solid volume fraction of 0.5. The friction coefficient μ is 0, the coefficient of restitution e is 0.95, and Young's modulus E is 8.7×10^9 Pa. Abbreviation: AR, aspect ratio. Figure reproduced with permission from Guo et al. (2013c).

2.2. Dense Flow

An interesting phenomenon in dense, sheared, granular flows is that flattened or elongated particles tend to align with their largest dimension in the shear flow direction (horizontal) and their smallest dimension in the velocity gradient direction (vertical) (**Figure 6**). The degree of particle alignment in a granular system can be described by an order parameter S, which is the largest eigenvalue of the symmetric traceless order tensor $\mathbf{Q}$ (Börzsönyi et al. 2012, Wegner et al. 2012):

$$Q_{ij} = \frac{3}{2N} \sum_{n=1}^{N} \left[\mathcal{L}_i^n \mathcal{L}_j^n - \frac{1}{3} \delta_{ij} \right],$$

where $\boldsymbol{\mathcal{L}}^n$ is the unit vector along the major axis of the cylindrical particle n, and the sum is over all N particles of interest. The order parameter S is equal to 1 if all the particles in the system are orientationally ordered in the same direction and is zero if the system is isotropic with a uniform distribution of particle orientation.

Figure 7 shows the variation of order parameter S with the maximum dimensional ratio of L/d_f and d_f/L, i.e., $\max(L/d_f, d_f/L)$, for dense flows at a solid volume fraction of $\nu = 0.5$. In general, S increases as the maximum dimensional ratio increases, indicating that the particle alignment becomes more significant as the particles become more elongated or flatter. For the frictionless particles, because of the alignment, the particles are allowed to flow in their own layers, minimizing interaction with their neighbors. As a result, smaller stresses are obtained for the more elongated or flatter particles without friction. However, sharp stress increases at higher solid volume fractions are observed for particles with friction, and this increase occurs at lower solid volume fraction values for more elongated or flatter particles (see **Figure 4**). Frictional

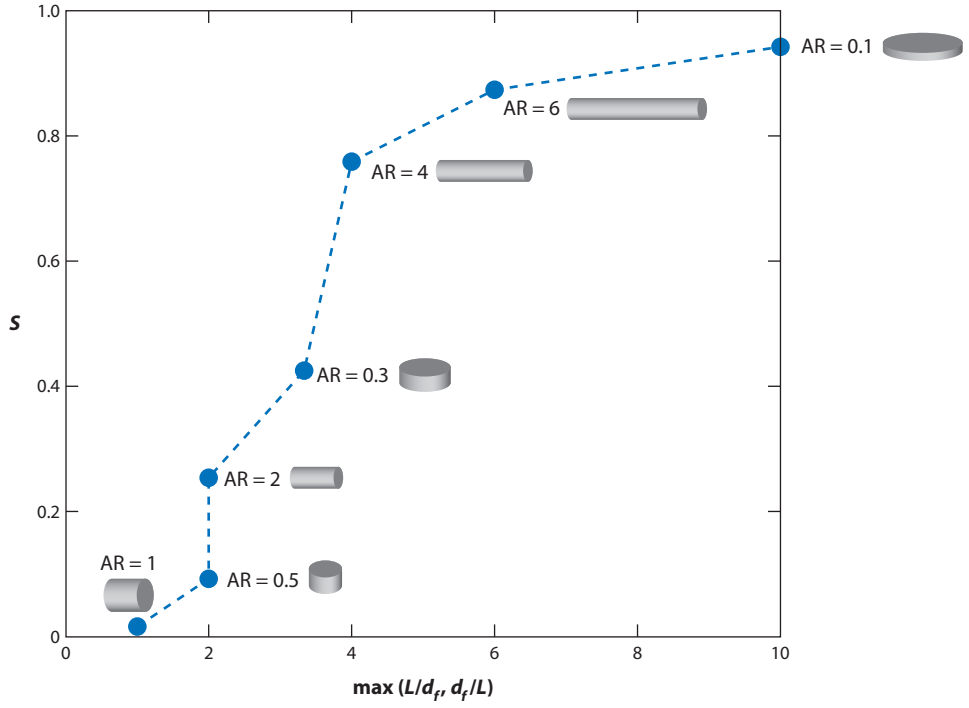

Figure 7

Variation of order parameter S with the maximum dimensional ratio of L/d_f and d_f/L for dense flows at the solid volume fraction of $\nu = 0.5$. The friction coefficient μ is 0, the coefficient of restitution e is 0.95, and Young's modulus E is 8.7×10^9 Pa. Abbreviation: AR, aspect ratio. Figure adapted with permission from Guo et al. (2013c).

forces promote the rotation of particles, and in dense flows, the particle rotation can increase the interparticle contacts, especially for elongated or flat particles owing to the presence of large dimensions. As the solid volume fraction increases, the effect of particle rotation on the contacts is counterbalanced by the effect of particle alignment, leading to the convergence of stresses at large solid volume fractions for the frictional particles of different aspect ratios (see **Figure 4**).

2.3. Quasi-Static Flow

DEM modeling has also been applied to systematically study the effect of particle shape on the quasi-static rheology of dense granular materials. In general, better connectivity (characterized by the coordination number) and larger shear strength (or the angle of internal friction) are obtained for more elongated particles (Azéma & Radjaï 2010, 2012; Peña et al. 2007), more angular polyhedra (Azéma et al. 2013, Langston et al. 2013), and flatter disks (Boton et al. 2013). The granular stresses are determined by the fabrics of interparticle contact forces and branch vectors that connect the mass centers of the particles in contact; the anisotropies of contact forces and branch vectors are strongly dependent on the particle shape. As shown in **Figure 8**, branch isotropy is observed for spherical particles with a platyness of $\eta = 0.0$; however, the anisotropy of normal and tangential components of branch vector $\boldsymbol{\ell}$ increases as the particles become flatter. The increase in anisotropy with the increasing particle platyness is also observed for the contact forces (Boton et al. 2013). Researchers have proposed mathematical expressions for the polar

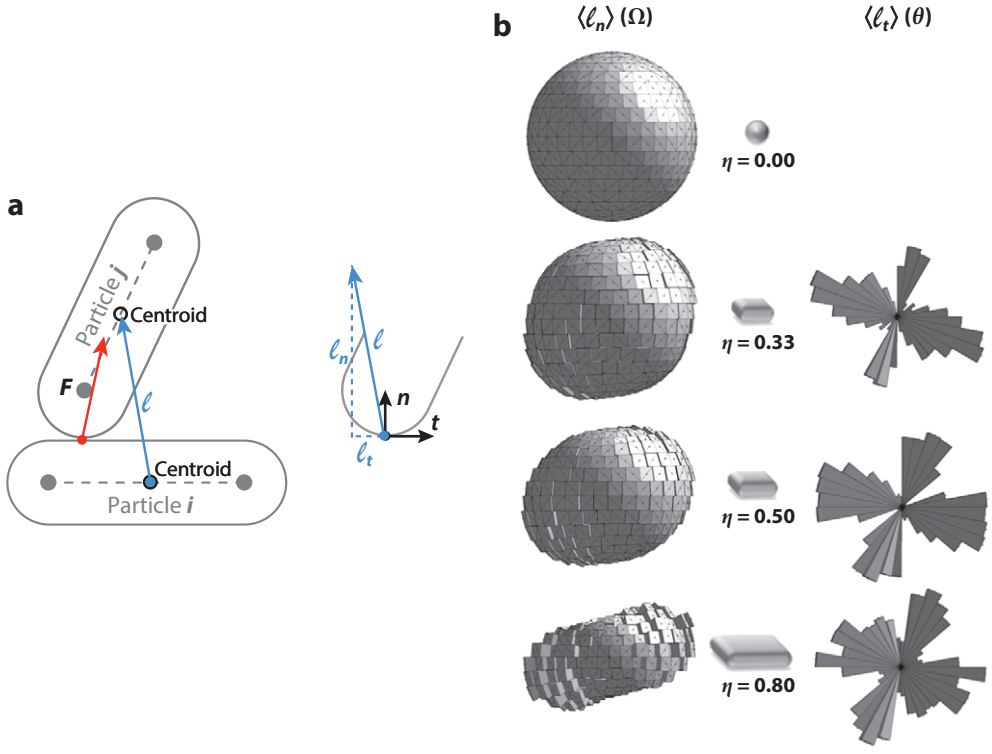

Figure 8

(*a*) An illustration of branch vector $\boldsymbol{\ell}$ and its components. (*b*) Polar distributions of average branch lengths in the normal direction $\langle \boldsymbol{\ell}_n \rangle$ and in the tangential direction $\langle \boldsymbol{\ell}_t \rangle$ for four sheared samples comprising particles of platyness $\eta = 0.00$, 0.33, 0.50, and 0.80. The definition of platyness η is provided by Boton et al. (2013), and larger values of η represent flatter particles. Figure adapted with permission from Boton et al. (2013).

distributions of contact forces and branch vectors and, subsequently, the internal friction angle as a function of particle elongation (Azéma & Radjaï 2012), angularity (Azéma et al. 2013), and platyness (Boton et al. 2013).

3. EFFECT OF PARTICLE FLEXIBILITY

To date, most DEM simulations have focused on rigid particles, which undergo negligible deformation in contacts. However, the effective handling of particulate materials such as biomass (e.g., corn stover and wheat straw), which is thought to be a future source of fuel, necessitates understanding the flow behavior of flexible particles for effective solid handling. Some DEM-based numerical models have been developed to investigate the dynamics of fibrous particles and fiber suspensions. As shown in **Figure 9**, flexible particles are represented in these models by chains of spheres (Kabanemi & Hétu 2012, Nguyen et al. 2013, Park & Kang 2009, Yamamoto & Matsuoka 1993), chains of prolate spheroids (Ross & Klingenberg 1997), or chains of short rods (Lindstrom & Uesaka 2007, Ning & Melrose 1999, Wang et al. 2006, Wu & Aidun 2010), which are connected by elastic bonds or ball-socket joints. Each pair of connected segments (spheres, spheroids, or rods) in a particle can bend and twist. The particle flexibility can be characterized by a bond stiffness, which is a function of the Young's modulus, shear modulus, and cross-sectional

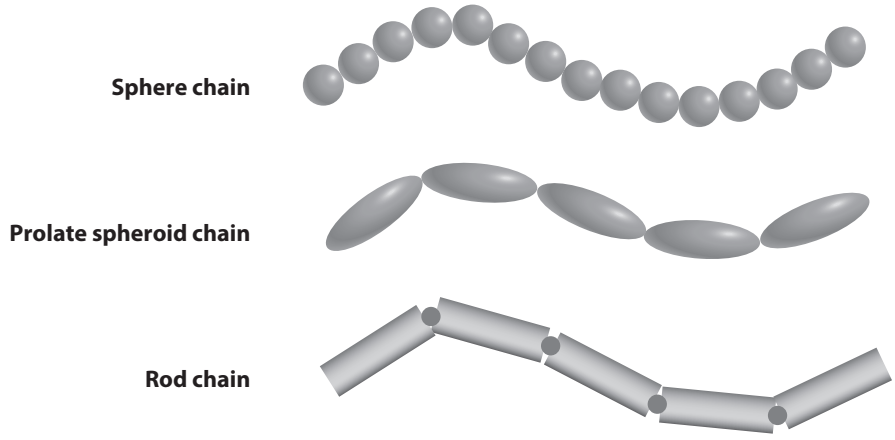

Figure 9

Various representations of a flexible fibrous particle in numerical simulations.

properties (area and area moment of inertia) of the bond. Efforts have also been made to validate the proposed flexible particle models. Nguyen et al. (2013) and Ning & Melrose (1999) verified the particle bending deformation and vibration by comparing them with the elastic beam bending theories. Guo et al. (2013d) verified their DEM model by a comprehensive examination of the static and dynamic behavior of particle bending, twisting, and stretching. Guo et al. (2013d) also proposed a time-step criterion to ensure numerical stability—that the time step should be less than the time it takes for an axial extensional/compressional wave to travel a single bond length.

As shown in **Figure 10**, a collinear collision between two flexible particles that have their major axes perpendicular to each other has been simulated using the flexible particle DEM model (Guo et al. 2013b). As the two particles bend during collision, kinetic energy is partially converted to potential energy. More kinetic energy is converted as the particles become more flexible (i.e., with smaller bond stiffness). Owing to the conversion of kinetic energy, a smaller coefficient of restitution is obtained for flexible particles compared to rigid particles, and the coefficient of restitution decreases as the particle flexibility increases. Unlike rigid particles, two flexible particles

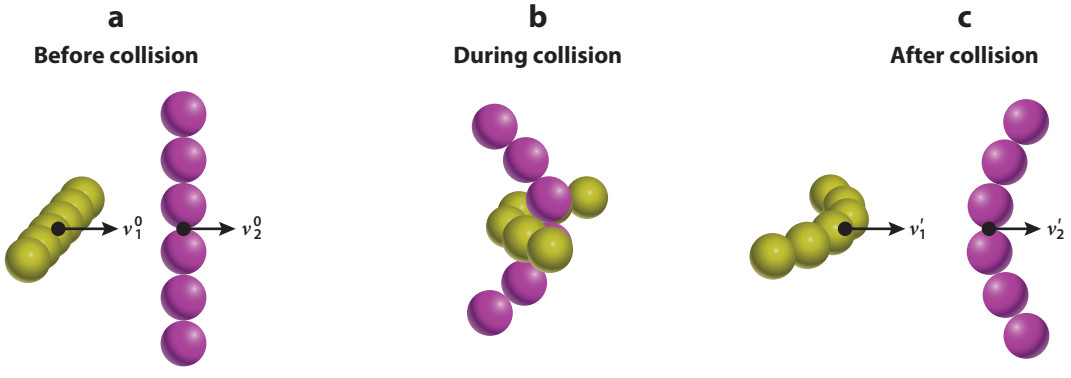

Figure 10

Snapshots (*a*) before, (*b*) during, and (*c*) after a collinear collision between two flexible fibers arranged with two major axes perpendicular to each other. Figure adapted with permission from Guo et al. (2013b).

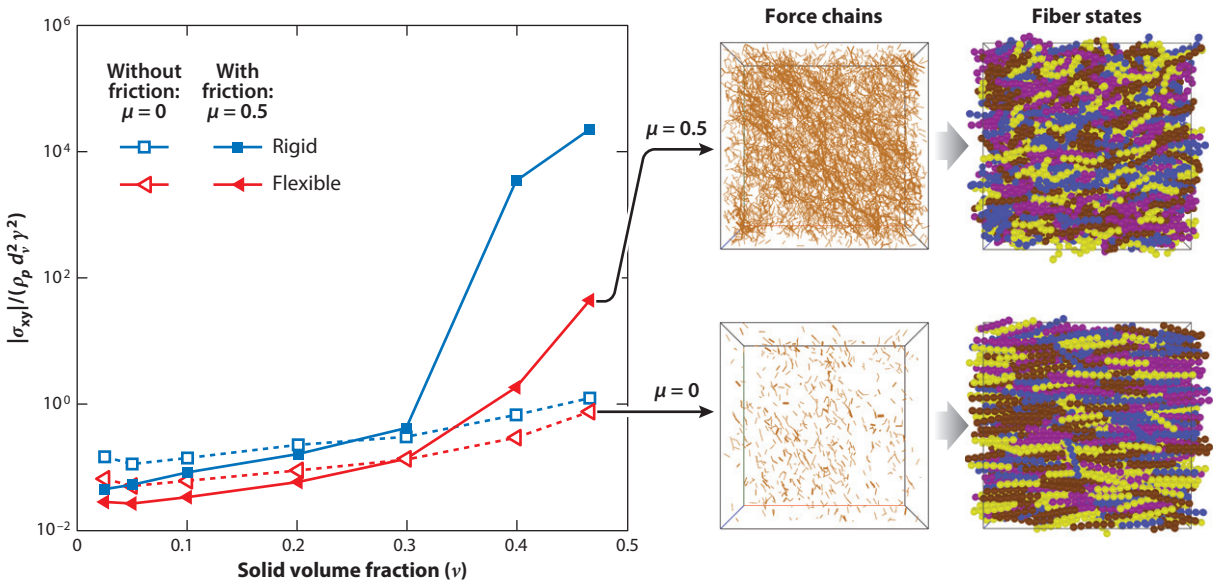

Figure 11

The normalized shear stress varying with the solid volume fraction in shear flows of rigid and flexible fibers with and without friction. The contact damping β_c is 1.63×10^{-2}, bond Young's modulus E_b is 2.6×10^4 Pa, and bond damping β_b is 0. Figure reproduced with permission from Guo et al. (2013a).

keep vibrating after the collision, and bond damping can be introduced to dissipate this energy in vibration.

Shear flows of flexible particles have also been modeled using the DEM (Guo et al. 2013a), and the shear stress results are shown in **Figure 11**. Compared to rigid particles, smaller stresses are obtained for the flexible particles, and a less sharp stress increase is observed at large solid volume fractions for the flexible particles with friction. For dense flows of frictionless, flexible particles (shown at $\nu = 0.47$), particle alignment occurs with the major axes aligned in the flow direction. As a result, the interparticle contacts are reduced, and particle deformation is minimized. For dense flows of flexible particles with friction $\mu = 0.5$, strong contacts are induced, and large particle deformation occurs.

In the sphere-chain flexible particle model, particle-particle contact is based on the interactions between two spheres. Therefore, one may introduce a liquid bridge force model (discussed below) for the contacts between spheres to the existing flexible particle model for the simulations of wet flexible particles. Thus, we recently simulated the shear flows of wet flexible particles (Y. Guo, J. Curtis, C. Wassgren, W. Ketterhagan & C. Hancock, unpublished data). As shown in **Figure 12**, agglomerates can be formed during the shear flow. Larger agglomerates are obtained for more flexible particles (with smaller bond Young's modulus) that undergo larger deformation.

4. PARTICLE BREAKAGE AND ATTRITION

In the industrial handling of bulk solids, particle breakage and attrition can occur through sliding, impact, and shear deformation. This breakage and attrition may lead to unwanted fines and change in material properties (flowability, packing, particle size distribution, and surface area), all of which can cause problems during subsequent delivery and further processing. Therefore, a

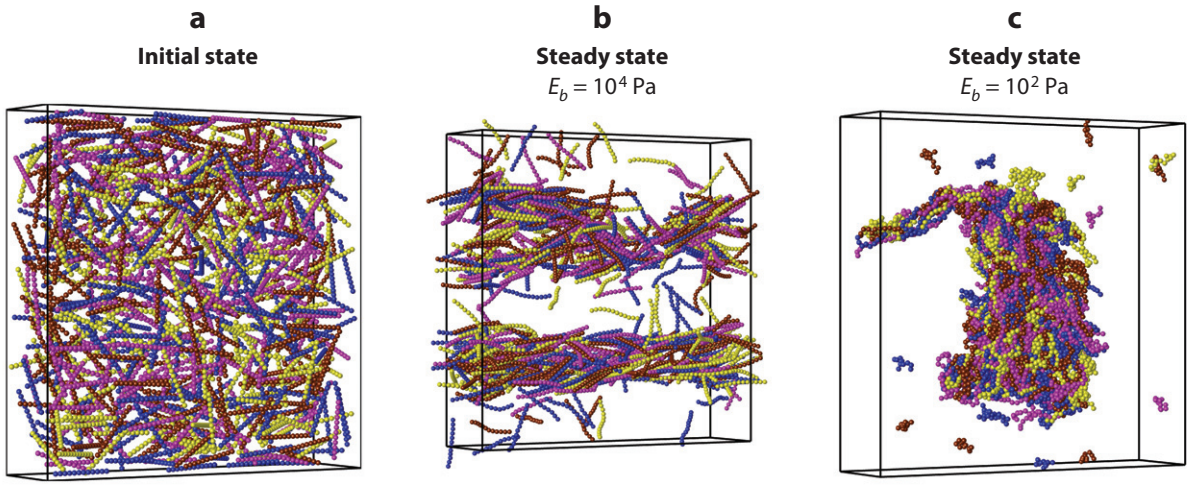

Figure 12

Shear flows of wet flexible fibers: (*a*) initial state, (*b*) steady state with bond Young's modulus of $E_b = 10^4$ Pa, and (*c*) steady state with $E_b = 10^2$ Pa.

good understanding of the breakage mechanism is crucial for process design optimization. DEM modeling has also been advanced and applied to the study of particle breakage and attrition, owing to the easy adjustment of controlling parameters and particle properties. Three major DEM models of particle breakage and attrition exist: the bonded-particle (BP), fragments spawning (FS), and attrition prediction (AP) models (**Figure 13**).

In the BP model, a particle or grain is formed by bonding a finite number of children particles, which can be spheres (Grof et al. 2007, Potyondy & Cundall 2004), squares (Potapov & Campbell 1997), or polygons (Hosseininia & Mirghasemi 2006). The breakage of a parent grain is modeled by the disconnection of bonded children particles as the stress in the bond exceeds the prescribed material strength (Potyondy & Cundall 2004). The BP model has been applied to simulate particle breakage under compaction (Grof et al. 2007, Hosseininia & Mirghasemi 2006) and shear (Potapov & Campbell 1997). A significant advantage of this model is that the stress distribution and fracture propagation within a particle can be obtained with a sufficient number of children particles. The drawback of this model is the limited size distribution of fragments, considering that a fragment consists of children particles. To increase the fragment size distribution, one may use more children particles to create a parent particle. However, the computational expense rises with the increase in the number of children particles.

To overcome the disadvantage of the limited fragment size distribution with the BP model, researchers proposed the FS model, allowing unlimited fragment size fractions, in principle (Brosh et al. 2011, Bruchmüller et al. 2011, Kalman et al. 2009). In this model, if the operating stress upon each collision is smaller than the strength of a particle, a fatigue function is implemented, and a reduced strength is assigned to the particle. Otherwise, if the operating stress is greater than the particle strength, the breakage function is implemented, and a mother spherical particle is then replaced by children spheres of a large size distribution. The generation of the children particles after breakage is governed by the specified fragments' spawning, seeding, and interaction algorithms, which lead to an empirical size distribution (obtained from real experiments) and guarantee the conservation of mass, momentum, and energy. The FS model has been successfully used to predict particle comminution in jet milling and pneumatic conveying (Brosh et al. 2011).

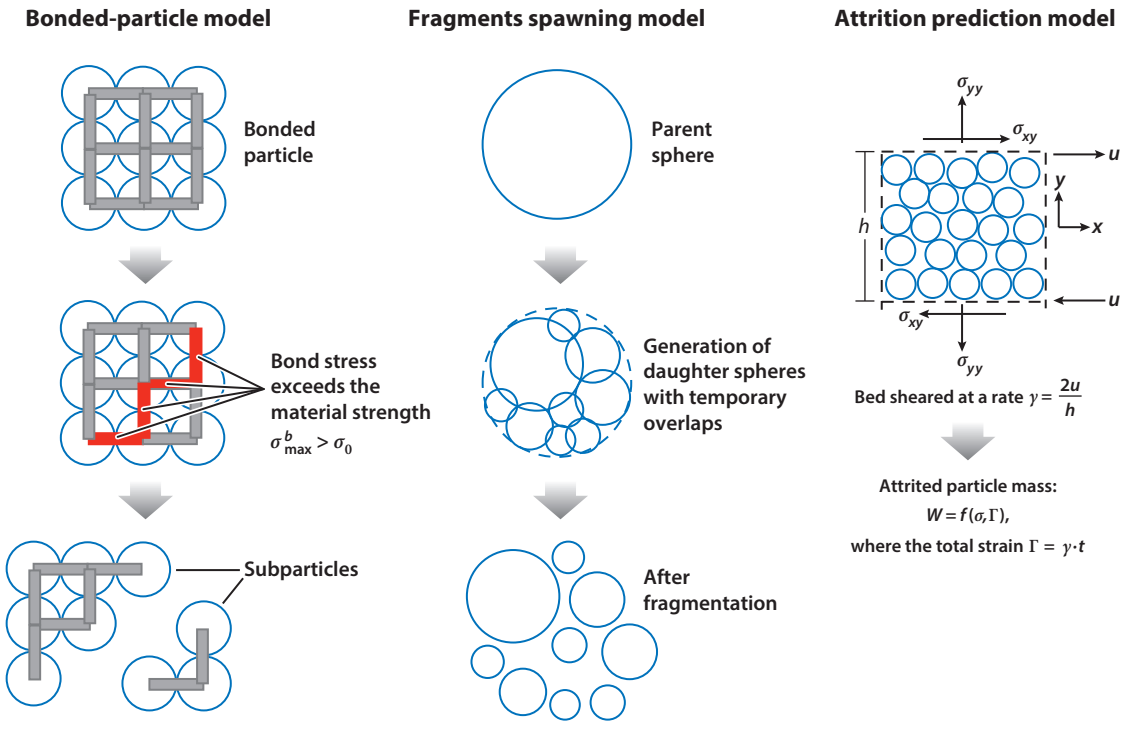

Figure 13

An illustration of three discrete element method–based approaches for the modeling of particle breakage and attrition.

Despite the advantage of its flexibility to produce any number and size distribution of fragments, several disadvantages with this approach exist: Its effective use heavily depends on the breakage function that is proposed empirically; the internal stress distribution and fracture propagation in a particle cannot be resolved; the current applications of FS models are limited to spherical particles, and nonspherical particles and fragments have not been described using these models.

Recently, Hare et al. (2011) proposed an AP model to predict the extent of particle attrition in agitated particle beds. In the AP model, the distributions of stresses and strains in the bed are estimated via DEM modeling. Then the extent of particle attrition is predicted from an empirical correlation between attrition and particle-phase stresses and strains. Such a correlation can be obtained experimentally from the shear cell tests (Neil & Bridgwater 1994). In this approach, the change in particle size due to breakage and attrition is not considered in the DEM modeling, and the attrited mass is computed based on the DEM outputs (i.e., stresses and strains). Therefore, the AP model may be applicable only to particle systems with a small extent of breakage and a small variation in the particle size distribution during the agitation process.

5. PARTICLE COHESION

Cohesive forces between particles may significantly affect particle packing behavior, the ease of particle transport and agglomeration, attrition, mixing, and erosive behaviors (Feng & Yu 1998, Henthorn & Hrenya 2009, Herminghaus 2005, Walton 2008). These effects can become particularly pronounced in the case of fine particulates (less than 100 μm) and are dependent on

the separation distance of the particles. We discuss three major sources of particle cohesion in this section: liquid induced, electrostatic, and van der Waals forces. In DEM simulations, these additional cohesive forces are merely added to the normal and tangential contact forces when the particles collide.

Simpler DEM treatments describe cohesion from any/all source(s) in a generic, lumped model that is not based on a specific physical interpretation. The linear cohesion model is one such example. Added to the contact model is a normal cohesive force that is the product of a constant cohesion energy density (the energy needed to remove a particle from its nearest neighbors divided by the total volume of the removed particle) multiplied by the contact area (Grima & Wypych 2011). Another example is the model of Weber & Hrenya (2006), who replaced the van der Waals potential with a square well potential (impulse force occurring at a preset particle separation distance). However, this type of treatment for describing cohesion requires the specification of the well depth and separation distance for force activation. In a similar fashion, Brewster et al. (2009) employed a Gaussian potential well to describe interparticle cohesive forces, and Jaeger et al. (2013), Waitukaitis et al. (2011), and Alexander et al. (2006) applied a constant-intensity normal force whenever particles are in contact.

Another approach in DEM simulations, often employed in geomechanics applications, is to incorporate mechanical models for the cohesive force based on macroscopic (bulk) characteristics of the granular materials using the Mohr-Coulomb failure criterion (Jiang et al. 2011, Tsuji et al. 2012, Utili & Nova 2008, Zhang & Li 2007). Here, model parameters are introduced, such as the intergranular friction angle and cohesive strength constant, which need experimental calibration for the DEM simulations to yield reliable quantitative predictions. More advanced DEM simulations incorporate detailed particle-level models for each individual type of cohesion, and these are discussed below.

5.1. Particle Cohesion by Liquid Bridging

When a film of liquid is introduced on the surface of particles, pendular liquid bridges form between the particles, resulting in an attractive capillary force that pulls them toward each other (Butt & Kappl 2009, Mitarai & Nori 2006, Simons 2007). This force can have a significant effect on the technology of granular systems. For example, hoppers that discharge smoothly in arid environments can clog in humid climates owing to liquid bridges between particles. As discussed by McCarthy (2009), liquid-induced cohesion can also significantly influence both segregation kinetics and the degree of segregation in particle mixtures. A representation of this is shown in **Figure 14** for the case of hopper discharge of a binary particle mixture with and without liquid-induced cohesion. Here, the degree of segregation decreases with increasing cohesion. In fact, the amount of moisture can be tuned to mitigate segregation without creating appreciable changes in hopper discharge rates (Anand et al. 2010).

The static, capillary force, F_{cap}, associated with a liquid bridge contains two components: (*a*) an axial component of the surface tension acting on the three-phase contact line (tensile term) and (*b*) the hydrostatic force due to the pressure deficiency in the bridge itself (Laplace term). In addition to the capillary force, particles are subject to a dynamic, viscous, enhanced resistance force, F_{visc}, resulting from a higher viscosity liquid (compared to the surrounding gas) filling the interstitial region between the particle surfaces. This force has a normal component, due to the radial pressure flow, and also a tangential component, due to the shear flow. DEM simulations with liquid bridging require descriptions for both the capillary and viscous forces, as well as the rupture distance, h_{rupture}, which is the maximum separation distance between the particles for which the liquid bridge is stable.

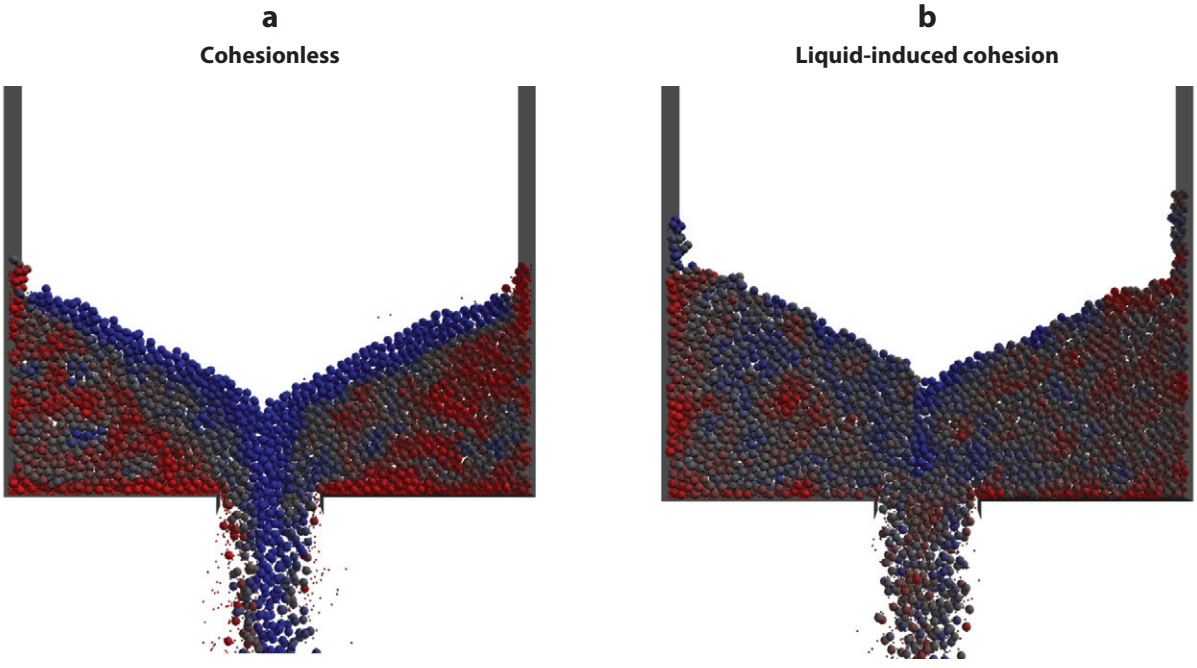

Figure 14

Discharge from a hopper with a binary particle mixture: (*a*) cohesionless and (*b*) liquid-induced cohesion with the Bond number (ratio of the maximum cohesive force to the gravitational force acting on a particle) equal to 1. Red and blue indicate large and small fines fractions, respectively, as compared to a well-mixed state (*gray*). Figure reproduced with permission from Anand et al. (2010).

Lian et al. (1993) derived the capillary force F_{cap} as a function of the half-filling angle ϕ, defined as $\phi = \tan^{-1}(r/R)$, where r is the radius of the liquid bridge, and R is the radius of the particle. However, to easily implement this capillary force into DEM simulations in a computationally efficient manner, one needs an explicit relationship between the capillary force and the liquid bridge volume and particle separation. From the solution of the Laplace-Young equation, describing the geometry of the liquid bridge, such relationships have been generated by Soulié et al. (2006), Willett et al. (2000), and Mikami et al. (1998). The analytical expressions of Soulié et al. (2006) for two unequal-sized spheres are given as

$$F_{\text{cap}} = \pi \gamma_{\text{st}} \sqrt{R_1 R_2} \left[\exp\left(A \frac{h}{R_2} + B \right) + C \right],$$

where

$$A = -1.1 \left(\frac{V}{R_2^3} \right)^{0.53},$$

$$B = \left(-0.148 \ln\left(\frac{V}{R_2^3} \right) - 0.96 \right) \beta^2 - 0.0082 \ln\left(\frac{V}{R_2^3} \right) + 0.48,$$

$$C = 0.0018 \ln\left(\frac{V}{R_2^3} \right) + 0.078,$$

γ_{st} is the surface tension of the liquid, R_1 and R_2 are the radii of the two spheres, β is the contact angle of the liquid with the particle, h is the separation distance, and V is the liquid volume associated

with the liquid bridge. The constants A, B, and C are dimensionless regression parameters. Other simplified capillary force models incorporated into DEM simulations include those that assume (*a*) a simple exponential decay expression for the capillary force in the case of two unequal-sized spheres (Richefeu et al. 2008), (*b*) an approximation of the shape of the liquid bridge as an arc of a circle (Muguruma et al. 2000), or (*c*) a complete wetted particle (Hsiau & Yang 2003, Lambert et al. 2008, Pitois et al. 2000).

Liquid bridges disappear when the particle separation increases to the point of bridge rupture. Experiments by Mason & Clark (1965) showed that the rupture distance for similar particles varies linearly with contact angle β and $V^{1/3}$. Additional theoretical considerations, as given by Lian et al. (1993), yielded the following specific relationship for the quasi-static rupture distance:

$$h_{\text{rupture}} = (1 + 0.5\beta)V^{1/3}.$$

Pitois et al. (2000) modified this rupture distance model to include the effect of the particle velocity. They showed that the dynamic rupture distance is larger than its static counterpart and increases with increasing capillary number, which is a function of the relative speed between the particles, the liquid viscosity, and the surface tension.

For the viscous force, the lubrication approximation and the elastohydrodynamic model in the case of two rigid spheres yield a closed-form expression for the dynamic viscous force in the normal direction:

$$F_{\text{visc}_n} = 6\pi\eta R^{*^2}\frac{v_n}{h},$$

where

$$\frac{1}{R^*} = \frac{1}{R_1} + \frac{1}{R_2},$$

η is the viscosity of the liquid, v_n is relative normal velocity between the particles, and R^* is the effective particle radius (Lian et al. 1998). Pitois et al. (2000) proposed a correction coefficient to this viscous force for cylindrical liquid bridges of finite liquid volume. The case of rigid sphere motion parallel to a planar wall is typically employed to describe the tangential viscous force (Nase et al. 2001). For sufficiently small separation distances, one finds

$$F_{\text{visc}_t} = \left(\frac{8}{15}\ln\frac{R^*}{h} + 0.9588\right)6\pi\eta R^* v_t,$$

where v_t is the relative tangential velocity between the particles. Although these descriptions predict an unbounded magnitude of the viscous force with infinitely small particle separation gaps, in practice, the surface roughness limits the approach of the spheres. Hence, a minimum value for h, corresponding to an average asperity height of the two surfaces, is taken, and the viscous force remains constant below this cutoff value.

When implementing liquid bridge force models into DEM simulations, one must make several assumptions regarding liquid distribution, bond formation, and bond rupture. The first is regarding the distribution of liquid. In the work of Muguruma et al. (2000), the total amount of liquid is distributed uniformly among all gaps smaller than the rupture distance. For binary particle systems, Richefeu et al. (2008) related the volume of liquid in the bond to the mean particle size, as the liquid retention capacity is greater for larger particles. Most commonly, the liquid is taken to be distributed evenly on the surface of all the particles, and every particle is assumed to have a constant thickness of liquid layer around it (Liu et al. 2011, 2013; Yang et al. 2003).

The second assumption deals with the amount of liquid held on the surface of each particle for a disparate particle mix. For bidisperse systems, Anand et al. (2010) took the ratio of the total amount of liquid on a larger particle d_l to that on the smaller particle d_s to be $(d_l/d_s)^2$. Their work

considered two sizes of particles of the same material, so the contact angle of the liquid with both particles is the same, and each particle carries the same initial amount of liquid during the entire course of the DEM simulation. However, Shi & McCarthy (2008) considered the more complex case of liquid transfer between particles of different materials with varying contact angles and the corresponding liquid redistribution upon bridge rupture. Experiments and modeling by Mani et al. (2012, 2013) also provided new insights into liquid redistribution due to shear and showed decreasing liquid content for pendular liquid bridges inside shear bands.

The third assumption regarding the implementation of liquid bridge force models into DEM simulations is the amount of liquid from each particle that takes part in bond formation. In some approaches, the volume of all the liquid bridges in the particle mixture is equal and constant (Kohonen et al. 2004, Zhu et al. 2013). The volume of the liquid bridge is estimated based on the particle size, the bridge coordination number, the ratio of the liquid volume to the total volume of dry particles, and the wet particle packing density. In the works of Liu et al. (2011, 2013), the liquid on each particle is equally divided (up to a specified maximum liquid bridge volume) among contact points when particles interact. Shi & McCarthy (2008) proposed that the liquid on the surface of each particle that is within the area of the spherical cap neighboring the contact spot contributes to the liquid bridge. That is, the bridge extracts liquid from the particle surfaces near the point of contact. The spherical cap is bounded by tangential lines from the center of one particle to the surface of the other particle. For virtually all DEM simulations that include liquid bridge forces, liquid bridges are assumed to slip over the particle surface, and the magnitude of the cohesive force remains constant during enduring contacts (overlapping particles).

5.2. Electrostatic Effects

Electrostatic forces resulting from charged or polarized particles/surfaces can cause profound changes in the structure of a granular flow field and can lead to particle clustering, blockages in granular flow, and dust explosions due to the accumulation of excessive electrostatic charges. These forces are especially problematic when handling insulating materials that do not readily dissipate charge. Alternatively, the addition of electrostatic forces can also lead to an increased collection of particles in filtration systems or electrostatic precipitators for dust mitigation. Confining wall material, particle composition, the relative humidity of the conveying fluid used, and the presence/absence of an antistatic agent in the system all influence the electrostatic charge generation characteristics and the observed flow patterns.

In the simplest treatment, electrostatic forces between two similarly charged particles or between a particle and an electric field are incorporated into DEM models through Coulomb's force and/or law, where the electrostatic force is included in Newton's second law along with the other forces acting on each particle (Lim et al. 2006, Nwose et al. 2012, Yang et al. 2012). The electrostatic force is given by

$$q E_e \quad \text{and/or} \quad \frac{q_1 q_2}{4\pi \varepsilon_o S^2},$$

where q is the particle charge, E_e is the strength of the electric field, S is the distance between the centers of charged particles 1 and 2, and ε_o is the vacuum permittivity. However, this simple model for two charged particles does not account for the effect of other charged particles in the region. Hence, a screening term is added to include this effect (Hogue et al. 2008). The screened Coulombic force is given by

$$\frac{q_1 q_2}{4\pi \varepsilon_o} \left(\frac{K}{S} + \frac{1}{S^2} \right) e^{-KS},$$

where K is the inverse of the Debye length and depends on the relative permittivity, the temperature, and local charge concentration. The screening term takes into consideration the number of particles of various charges within a specified screening distance from the target particle.

More complex treatments consider contributions from both the dielectrophoretic force and the Coulombic force to describe the total electric force experienced by a particle. The dielectrophoretic force is equal to the dot product of the electric field gradient and the dipole moment, comprising any permanent dipole moment and dipoles induced by the electric field. The induced dipole moment is a function of the electric field, the particle diameter, and the fluid and particle dielectric permittivities. The electric field is the aggregate of the electric field induced by the particles themselves and the applied electric field. Electric torques on the particle, induced by interactions with the electric field, must also be included, unless the particles have no permanent dipole or the induced dipole is aligned with the electric field. Park & Park (2005) employed this modeling approach for DEM simulations of particle deposition when an electric field is applied across a fibrous filter. In this case, a particle passing through the filter experiences a Coulombic force, which includes contributions from the electric field around a fiber and the electric fields around all the deposited particles. Additionally, a dielectrophoretic force is included that accounts for contributions due to polarization between the passing particle and both the fiber and all the deposited particles. However, this method becomes computationally expensive as the number of particles increases. Hence, for a similar filtration operation, Yang et al. (2013b) employed a combined boundary element method and multi-pole-expansion approach that accounts for the general electrostatic field and electrostatic forces for all the particles. This same type of treatment has been employed to mitigate dust adhesion and transport particles away from a surface using traveling waves on an electric curtain (Liu & Marshall 2010, Liu et al. 2010).

Some DEM simulations have included the effect of triboelectric charging (tribocharging) in which particles of different material and effective work function collide, causing an exchange of charge, or particles gain/dissipate electrical charge when they come into contact with a confining wall. Hogue et al. (2008) considered the tribocharging of glass beads as they roll, slide, and bounce down various inclined planes made from different materials. They describe the resulting charge transfer via an equation of charge as a function of time, which includes the saturation charge and a material-dependent time constant for charge generation (dissipation is neglected), which is determined experimentally. Hogue et al. (2009) expanded their treatment of the particle-plane tribocharging effect to include the initial charge on the particle and an approximation for the electrostatic force between the charged particle and the charged planar surface. Imba et al. (2013) described the tribocharging of initially neutral particles in a shaker in a different manner than did Hogue et al. (2009). When a particle hits the shaker walls, the amount of transferred charge in each collision depends on the maximum contact area (calculated based on the maximum overlap), a proportionality constant, and the charge on the particle as it approaches the saturation charge. Supuk et al. (2011) discussed a relationship between these two different treatments; for a long timescale, the integrated maximum contact area is proportional to the time of the tribocharging operation.

5.3. Van der Waals Forces

Van der Waals forces, F_{vdw}, result from intermolecular forces, and the magnitude of their force between two spheres is given by

$$F_{\text{vdw}} = \frac{AR_c}{6b^2},$$

where R_c is the contact radius, and A is the Hamaker constant (on the order of 10^{-20} J for solids in air). Israelachvili (1992) gave values for the Hamaker constant for varying geometries and materials.

Van der Waals forces can be large at very small separation distances or when particles are in contact but decrease rapidly with increasing separation distance. Although they are always present, they can typically be neglected for particles larger than a few hundred micrometers. For rough particles, the magnitude of the van der Waals force is dependent on the local radius of curvature of surface asperities on the particle rather than on the size of the particle itself (Prokopovich & Starov 2011, Seville et al. 2000).

In DEM simulations, some researchers have directly added the van der Waals force to the contact force in the balance of forces acting on the particle (Sanchez & Scheeres 2013; Tatemoto et al. 2005; Yang et al. 2008a,b; Ye et al. 2004). In these cases, a cutoff value for the interparticle distance must be defined to avoid the numerical singularity at particle contact. However, the van der Waals force also interacts with the other contact forces, so it should not simply be added to the force balance. Instead, contact models incorporating the effect of the van der Waals force (often called adhesive contact models) should be employed. O'Sullivan (2011), Fischer-Cripps (2007), and Tomas (2007a) have compiled detailed listings of common normal and tangential contact models that incorporate adhesion.

Elastic, adhesive normal contact models employed in DEM simulations are the JKR and DMT models for smooth spherical particles (Johnson et al. 1971, Derjaguin et al. 1975), with JKR being the more commonly used of the two. The JKR model acts only over the contact area and is appropriate for soft materials with high surface energy. The DMT model is more suitable for hard materials with low surface energy and accounts for forces outside the contact area. In these models, there is a critical, pull-off force to separate the two particles; this pull-off force is dependent on the surface energy of the particles. The Tabor parameter, which is the ratio of the range of the surface force to the elastic deformation, gives a measure of the transition between these two regimes; the JKR model should be used for high values of the Tabor parameter. DEM simulations based on the JKR model are often used to investigate particle mixing, breakage, and agglomeration for fine particles (Calvert et al. 2013, Figueroa et al. 2009, Marshall 2009, Moreno-Atanasio 2012, Yang et al. 2013a).

Adhesive normal contact models including plasticity have been developed by Thornton & Ning (1998), Tomas (2007a,b), Luding (2008), Luding & Alonso-Marroquín (2011), and Walton & Johnson (2009). In the model of Thornton & Ning (1998), the resulting larger contact region upon unloading and the larger pull-off force are described by a modified JKR model with a larger contact radius. Tomas (2007a,b) proposed an elaborate model, involving six material parameters, which includes nonlinear-elastic and linear-plastic loading, plasticity with energy dissipation, and adhesion. The Luding (2008; Luding & Alonso-Marroquín 2011) model is a simplified version of the Tomas model that neglects the Hertzian, elastic regime and includes five parameters (Tykhoniuk et al. 2007). Walton & Johnson (2009) accounted for the torsion and bending strength that may exist between adhesive particles, and their model involves eight parameters. The effect of adhesion on the tangential sliding force was examined by Savkoor & Briggs (1977), who incorporated the JKR model into tangential contact mechanics by varying the contact radius. Thornton & Yin (1991) modified this model to include a smoothly varying contact radius until the onset of sliding.

6. CONCLUDING REMARKS

The DEM allows for a more in-depth study of granular flows than is often feasible using experimentation—in particular, when probing the interior of granular flows is required. Commonly, DEM simulations are tested at the level of macro (bulk) behavior. More recent research has been aimed at detailed and nonintrusive particle-level measurements to quantitatively validate the DEM. For example, new physical understanding at the microlevel of wet particle collisions

resulting in agglomeration or deagglomeration holds promise for potentially simplifying and improving DEM models of wet, dense granular flows (e.g., Donahue et al. 2012, Kantak et al. 2009).

DEM simulations including particle cohesion due to liquid bridging and van der Waals forces have been more rigorously investigated, whereas electrostatic interactions have received relatively less attention. However, even the most rigorous liquid bridging models involve simplifications, such as in the descriptions for the dynamic normal and tangential viscous forces. The significance of these simplifications, in terms of reliably simulating practical flows, has yet to be determined. Also, in the adhesive contact models, problems exist when relating model parameters to bulk material properties, such as calibrating surface energy parameters from atomic force microscopy studies (likely because of detailed particle surface morphology effects). In addition, there is a notable lack of DEM simulations that currently involve combinations of cohesive mechanisms. For example, if moisture is added to a granular system to reduce cohesion due to electrostatic charging, it can also increase cohesion due to liquid bridging or lubricate the friction between solids. Another situation is the presence of moisture significantly modifying the van der Waals force on the particle by changing the effective Hamaker constant and increasing the separation distance between the interacting particles. More DEM simulations investigating these phenomena are needed.

Despite these challenges, there is a bright future for DEM modeling. DEM simulations can provide particle stress information that can develop or validate particle models that describe the particle phase as a continuum. This has been demonstrated for the case of nonspherical grains. Such a multiscale approach is particularly attractive for particulate systems in which constitutive relations are difficult to develop from fundamental principles. In addition, as computational capability expands, the scope and diversity of systems that can be modeled by the DEM broaden. Hence, other problems, such as those associated with the limited size of systems that can be currently modeled, can be eliminated. These include the description of a realistic particle size distribution, the number of constituent spheres needed to mimic an actual particle surface, and the system-size dependence of the extracted transport coefficients that are needed for the development of closure models.

DISCLOSURE STATEMENT

The authors are not aware of any biases that might be perceived as affecting the objectivity of this review.

ACKNOWLEDGMENTS

We are grateful for the support of the National Science Foundation (NSF), grant 0854005; the State of Florida Space Research Initiative; and the NSF I/UCRC Center for Particulate and Surfactant Systems, grant 0749481/0749461, as well as the ongoing support of its industry members.

LITERATURE CITED

Alexander AW, Chaudhuri B, Faqih A, Muzzio FJ, Davies C, Tomassone MS. 2006. Avalanching flow of cohesive powders. *Powder Technol.* 164:13–21

Anand A, Curtis J, Wassgren C, Hancock B, Ketterhagen W. 2010. Segregation of cohesive granular materials during discharge from a rectangular hopper. *Granul. Matter* 12:193–200

Azéma E, Radjaï F. 2010. Stress-strain behavior and geometrical properties of packings of elongated particles. *Phys. Rev. E* 81:051304

Azéma E, Radjaï F. 2012. Force chains and contact network topology in sheared packings of elongated particles. *Phys. Rev. E* 85:031303
Azéma E, Radjaï F, Dubois F. 2013. Packings of irregular polyhedral particles: strength, structure, and effects of angularity. *Phys. Rev. E* 87:062203
Barker GC. 1994. Computer simulations of granular materials. In *Granular Matter: An Interdisciplinary Approach*, ed. A Mehta, pp. 35–83. New York: Springer-Verlag
Börzsönyi T, Szabo B, Toros G, Wegner S, Torok J, et al. 2012. Orientational order and alignment of elongated particles induced by shear. *Phys. Rev. Lett.* 108:228302
Boton M, Azéma E, Estrada N, Radjaï F, Lizcano A. 2013. Quasistatic rheology and microstructural description of sheared granular materials composed of platy particles. *Phys. Rev. E* 87:032206
Brewster R, Grest GS, Levine AJ. 2009. Effects of cohesion on the surface angle and velocity profiles of granular material in a rotating drum. *Phys. Rev. E* 79:011305
Brosh T, Kalman H, Levy AJ. 2011. Fragments spawning and interaction models for DEM breakage simulation. *Granul. Matter* 13:765–76
Bruchmüller J, van Wachem BGM, Gu S, Luo KH. 2011. Modelling discrete fragmentation of brittle particles. *Powder Technol.* 208:731–39
Butt HJ, Kappl M. 2009. Normal capillary forces. *Adv. Colloid Interface Sci.* 146:48–60
Calvert G, Hassanpour A, Ghadiri M. 2013. Analysis of aerodynamic dispersion of cohesive clusters. *Chem. Eng. Sci.* 86:146–50
Campbell C. 1990. Rapid granular flows. *Annu. Rev. Fluid Mech.* 22:57–92
Campbell C. 2006. Granular material flows: an overview. *Powder Technol.* 162:208–29
Campbell C. 2011. Elastic granular flows of ellipsoidal particles. *Phys. Fluids* 23:013306
Cleary P. 2008. The effect of particle shape on simple shear flows. *Powder Technol.* 179:144–63
Cundall PA, Strack ODL. 1979. A discrete numerical model for granular assemblies. *Géotechnique* 29:47–65
Derjaguin BV, Muller VM, Toporov YP. 1975. Effect of contact deformations on the adhesion of particles. *J. Colloid Interface Sci.* 53:314–26
Donahue CM, Davis RH, Kantak AA, Hrenya CM. 2012. Mechanisms for agglomeration and deagglomeration following oblique collisions of wet particles. *Phys. Rev. E* 86:021303
Feng CL, Yu AB. 1998. Effect of liquid addition on the packing of mono-sized coarse spheres. *Powder Technol.* 99:22–28
Figueroa I, Li H, McCarthy J. 2009. Predicting the impact of adhesive force on particle mixing and segregation. *Powder Technol.* 195:203–12
Fischer-Cripps AC. 2007. *Introduction to Contact Mechanics*. New York: Springer. 2nd ed.
Forterre Y, Pouliquen O. 2008. Flows of dense granular media. *Annu. Rev. Fluid Mech.* 40:1–24
Goldhirsch I. 2003. Rapid granular flows. *Annu. Rev. Fluid Mech.* 35:267–93
Grima A, Wypych PW. 2011. Development and validation of calibration methods for discrete element modelling. *Granul. Matter* 13:127–32
Grof Z, Kohout M, Štěpánek F. 2007. Multi-scale simulation of needle-shaped particle breakage under uniaxial compaction. *Chem. Eng. Sci.* 62:1418–29
Guises R, Xiang J, Latham JP, Munjiza A. 2009. Granular packing: numerical simulation and the characterization of the effect of particle shape. *Granul. Matter* 11:281–92
Guo Y, Wassgren C, Ketterhagen W, Hancock B, James B, Curtis J. 2012. A numerical study of granular shear flows of rod-like particles using the discrete element method. *J. Fluid Mech.* 713:1–26
Guo Y, Curtis J, Wassgren C, Hancock C, Ketterhagan W. 2013a. Discrete element modeling of granular shear flows and breakage of flexible fibers. *Proc. 6th Int. Conf. Discrete Element Methods Relat. Tech.* (*DEM6*), ed. G Mustoe, pp. 349–54. Golden, CO: Colo. Sch. Mines
Guo Y, Curtis J, Wassgren C, Ketterhagan W, Hancock C. 2013b. Granular shear flows of flexible rod-like particles. *Powders Grains: Proc. 7th Int. Conf. Micromech. Granul. Media*, pp. 491–94. College Park, MD: Am Inst. Phys.
Guo Y, Wassgren C, Hancock B, Ketterhagen W, Curtis J. 2013c. Granular shear flows of flat disks and elongated rods without and with friction. *Phys. Fluids* 25:063304
Guo Y, Wassgren C, Hancock B, Ketterhagen W, Curtis J. 2013d. Validation and time step determination of discrete element modeling of flexible fibers. *Powder Technol.* 249:386–95

Hare C, Ghadiri M, Dennehy R. 2011. Prediction of attrition in agitated particle beds. *Chem. Eng. Sci.* 66:4757–70

Henthorn KH, Hrenya CM. 2009. Particle cohesion. In *Encyclopedia of Chemical Processing*, ed. S Lee.London: Taylor & Francis. doi: 10.1081/E-ECHP-120044868

Herminghaus S. 2005. Dynamics of wet granular matter. *Adv. Phys.* 54:221–61

Hogue MD, Calle CI, Curry DR, Weitzman PS. 2009. Discrete element method (DEM) of triboelectrically charged particles: revised experiments. *J. Electrostat.* 67:691–94

Hogue MD, Calle CI, Weitzman PS, Curry DR. 2008. Calculating the trajectories of triboelectrically charged particles using Discrete Element Modeling (DEM). *J. Electrostat.* 66:32–38

Hosseininia ES, Mirghasemi AA. 2006. Numerical simulation of breakage of two-dimensional polygon-shaped particles using discrete element method. *Powder Technol.* 166:100–12

Hsiau S-S, Yang S-C. 2003. Numerical simulation of self-diffusion and mixing in a vibrated granular bed with the cohesive effect of liquid bridges. *Chem. Eng. Sci.* 58:339–51

Imba M, Kanazawa T, Ida J, Yamamoto H, Ghadiri M, Matsuyama T. 2013. Tribo-electric charging particle in a shaker. *AIP Conf. Proc.* 1542:90–92

Israelachvili J. 1992. *Intermolecular and Surface Forces*. New York: Academic. 2nd ed.

Jaeger HM, Miskin MZ, Waitukaitis SR. 2013. From nanoscale cohesion to macroscale entanglement: opportunities for designing aggregate behavior by tailoring grain shape and interactions. *AIP Conf. Proc.* 1542:3–6

Jenkins J. 2006. Dense shearing flows of inelastic disks. *Phys. Fluids* 18:103307

Jiang MJ, Yan HB, Zhu HH, Utili S. 2011. Modeling shear behavior and strain localization in cemented sands by two-dimensional distinct element method analyses. *Comput. Geotech.* 38:14–29

Johnson KL, Kendall K, Roberts AD. 1971. Surface energy and the contact of elastic solids. *Proc. R. Soc. A* 324:301–13

Kabanemi KK, Hétu JF. 2012. Effects of bending and torsion rigidity on deformation and breakage of flexible fibers: a direct simulation study. *J. Chem. Phys.* 136:074903

Kalman H, Rodnianski V, Haim M. 2009. A new method to implement comminution functions into DEM simulation of a size reduction system. *Granul. Matter* 11:253–66

Kantak AA, Hrenya CM, Davis RH. 2009. Initial rates of aggregation for dilute, granular flows of wet particles. *Phys. Fluids* 21:023301

Katagiri J, Matsushima T, Yamada Y. 2010. Simple shear simulation of 3D irregularly-shaped particles by image-based DEM. *Granul. Matter* 12:491–97

Kodam M, Bharadwaj R, Curtis J, Hancock B, Wassgren C. 2010. Cylindrical object contact detection for use in discrete element method simulations. Part 1: contact detection algorithms. *Chem. Eng. Sci.* 65:5852–62

Kohonen MM, Geromichalos D, Scheel M, Schier C, Herminghaus S. 2004. On capillary bridges in wet granular materials. *Physica A* 339:7–15

Kruggel-Emden H, Simsek E, Rickelt S, Wirtz S, Scherer V. 2007. Review and extension of normal force models for the Discrete Element Method. *Powder Technol.* 171:157–73

Krumbein WC, Pettijohn FJ. 1938. *Manual of Sedimentary Petrography*. New York: Appleton-Century

Lambert P, Chau A, Delchambre A, Regnier S. 2008. Comparison between two capillary forces models. *Langmuir* 24:3157–63

Langston P, Ai J, Yu H-S. 2013. Simple shear in 3D DEM polyhedral particles and in a simplified 2D continuum model. *Granul. Matter* 15:595–606

Lees G. 1964. A new method for determining the angularity of particles. *Sedimentology* 3:2–21

Li S, Marshall J, Liu G, Yao Q. 2011. Adhesive particulate flow: the discrete element method and its application in energy and environmental engineering. *Prog. Energy Combust. Sci.* 37:633–68

Lian G, Thornton C, Adams MJ. 1993. A theoretical study of the liquid bridge forces between two rigid spherical bodies. *J. Colloid Interface Sci.* 161:138–47

Lian G, Thornton C, Adams MJ. 1998. Discrete particle simulation of agglomerate impact coalescence. *Chem. Eng. Sci.* 53:3381–91

Lim EWC, Zhang Y, Wang CH. 2006. Effects of an electrostatic field in pneumatic conveying of granular materials through inclined and vertical pipes. *Chem. Eng. Sci.* 61:7889–908

Lindstrom SB, Uesaka T. 2007. Simulation of the motion of flexible fibers in viscous fluid flow. *Phys. Fluids* 19:113307
Liu G, Marshall J. 2010. Effect of particle adhesion and interactions on motion by traveling waves on an electric current. *J. Electrostat.* 68:179–89
Liu G, Marshall J, Li S, Yao Q. 2010. Discrete element method for particle capture by a body in an electrostatic field. *Int. J. Numer. Methods Eng.* 84:1589–612
Liu PY, Yang RY, Yu AB. 2011. Dynamics of wet particles in rotating drums: effect of liquid surface tension. *Phys. Fluids* 23:013304
Liu PY, Yang RY, Yu AB. 2013. DEM study of the transverse mixing of wet particles in rotating drums. *Chem. Eng. Sci.* 86:99–107
Luding S. 2008. Cohesive, frictional powders: contact models for tension. *Granul. Matter* 10:235–46
Luding S, Alonso-Marroquín F. 2011. The critical-state yield stress (termination locus) of adhesive powders from a single numerical experiment. *Granul. Matter* 13:109–19
Mani R, Kadau D, Or D, Herrmann HJ. 2012. Fluid depletion in shear bands. *Phys. Rev. Lett.* 109:248001
Mani R, Kadau D, Or D, Herrmann HJ. 2013. On liquid migration in sheared granular matter. *AIP Conf. Proc.* 1542:499–502
Marshall JS. 2009. Discrete element method modeling of particulate aerosol flows. *J. Comput. Phys.* 228:1541–61
Mason G, Clark WC. 1965. Liquid bridges between spheres. *Chem. Eng. Sci.* 20:859–66
McCarthy J. 2009. Turning the corner in segregation. *Powder Technol.* 192:137–42
Mikami T, Kamiya H, Horio M. 1998. Numerical simulation of cohesive powder behavior in a fluidized bed. *Chem. Eng. Sci.* 53:1927–40
Mishra BK. 2003. A review of computer simulation of tumbling mills by the discrete element method: Part I—contact mechanics. *Int. J. Miner. Process.* 71:73–93
Mitarai N, Nori F. 2006. Wet granular materials. *Adv. Phys.* 55:1–45
Moreno-Atanasio R. 2012. Energy dissipation in agglomerates during normal impact. *Powder Technol.* 223:12–18
Muguruma Y, Tanaka T, Tsuji Y. 2000. Numerical simulation of particulate flow with liquid bridge between particles (simulation of centrifugal tumbling granulator). *Powder Technol.* 109:49–57
Nase ST, Vargas WL, Adetola AA, McCarthy JJ. 2001. Discrete characterization tools for cohesive granular material. *Powder Technol.* 116:214–23
Neil AU, Bridgwater J. 1994. Attrition of particulate solids under shear. *Powder Technol.* 80:207–19
Nguyen DH, Kang N, Park J. 2013. Validation of partially flexible rod model based on discrete element method using beam deflection and vibration. *Powder Technol.* 237:147–52
Ning Z, Melrose JR. 1999. A numerical model for simulating mechanical behavior of flexible fibers. *J. Chem. Phys.* 111:10717–26
Nwose EN, Pei C, Wu CY. 2012. Modelling die filling with charged particles using DEM/CFD. *Particuology* 10:229–35
O'Sullivan C. 2011. *Particulate Discrete Element Modelling: A Geomechanics Perspective*. London: Taylor & Francis
Park HS, Park YO. 2005. Simulation of particle deposition on filter fiber in an external electric field. *Korean J. Chem. Eng.* 22:303–14
Park J, Kang N. 2009. Applications of fiber models based on discrete element method to string vibration. *J. Mech. Sci. Technol.* 23:372–80
Peña AA, García-Rojo R, Herrmann HJ. 2007. Influence of particle shape on sheared dense granular media. *Granul. Matter* 9:279–91
Pitois O, Moucheront P, Chateau X. 2000. Liquid bridge between two moving spheres: an experimental study of viscosity effects. *J. Colloid Interface Sci.* 231:26–31
Potapov AV, Campbell CS. 1997. Computer simulation of shear-induced particle attrition. *Powder Technol.* 94:109–22
Potyondy DO, Cundall PA. 2004. A bonded-particle model for rock. *Int. J. Rock Mech. Min. Sci.* 41:1329–64
Prokopovich P, Starov V. 2011. Adhesion models: from single to multiple asperity contacts. *Adv. Colloid Interface Sci.* 168:210–22

Richefeu V, Youssoufi MSE, Peyroux R, Radjaï F. 2008. A model of capillary cohesion for numerical simulations of 3D polydisperse granular media. *Int. J. Numer. Anal. Methods Geomech.* 32:1365–83

Ross RF, Klingenberg DJ. 1997. Dynamic simulation of flexible fibers composed of linked rigid bodies. *J. Chem. Phys.* 106:2949–60

Sanchez DP, Scheeres DJ. 2013. Granular cohesion and fast rotators in the NEA population. *AIP Conf. Proc.* 1542:955–58

Savkoor AR, Briggs GAD. 1977. The effect of the tangential force on the contact of elastic solids in adhesion. *Proc. R. Soc. A* 356:103–14

Seville JPK, Willett CD, Knight PC. 2000. Interparticle forces in fluidisation: a review. *Powder Technol.* 113:261–68

Shi D, McCarthy JJ. 2008. Numerical simulation of liquid transfer between particles. *Powder Technol.* 184:64–75

Simons SJR. 2007. Liquid bridges in granules. In *Handbook of Powder Technology*, Vol. 11, ed. AD Salman, MJ Hounslow, JPK Seville, pp. 1257–316. Amsterdam: Elsevier

Soulié F, Cherblanc F, El Youssoufi MS, Saix C. 2006. Influence of liquid bridges on the mechanical behaviour of polydisperse granular materials. *Int. J. Numer. Anal. Methods Geomech.* 30:213–28

Supuk E, Hassanpour A, Ahmadian H, Ghadiri M, Matsuyama T. 2011. Tribo-electrification and associated segregation of pharmaceutical bulk powders. *KONA Powder Part. J.* 29:208–23

Tafesse S, Fernlund JMR, Sun W, Bergholm F. 2012. Evaluation of image analysis methods used for quantification of particle angularity. *Sedimentology* 60:1100–10

Tatemoto Y, Mawatari Y, Noda K. 2005. Numerical simulation of cohesive particle motion in a vibrated fluidized bed. *Chem. Eng. Sci.* 60:5010–21

Thornton C. 1999. Future developments in discrete element approaches: an introduction. In *Mechanics of Granular Materials*, ed. M Oda, K Iwashita, pp. 217–19. Boca Raton, FL: CRC

Thornton C, Ning Z. 1998. A theoretical model for the stick/bounce behaviour of adhesive, elastic-plastic spheres. *Powder Technol.* 99:154–62

Thornton C, Yin KK. 1991. Impact of elastic spheres with and without adhesion. *Powder Technol.* 65:153–66

Tomas J. 2007a. Adhesion of ultrafine particles: a micromechanical approach. *Chem. Eng. Sci.* 62:1997–2010

Tomas J. 2007b. Adhesion of ultrafine particles: energy absorption at contact. *Chem. Eng. Sci.* 62:5925–39

Tsuji T, Nakagawa Y, Matsumoto N, Kadono Y, Takayama T, Tanaka T. 2012. 3-D DEM simulation of cohesive soil-pushing behavior by bulldozer blade. *J. Terramech.* 49:37–47

Tykhoniuk R, Tomas J, Luding S, Kappl M, Heim LO, Butt HJ. 2007. Ultrafine cohesive powders: from interparticle contacts to continuum behaviour. *Chem. Eng. Sci.* 62:2843–64

Utili S, Nova R. 2008. DEM analysis of bonded granular geomaterials. *Int. J. Numer. Anal. Methods Geomech.* 32:1997–2031

Waitukaitis SR, Grütjen H, Royer JR, Jaeger HM. 2011. Droplet and cluster formation in freely falling granular streams. *Phys. Rev. E* 83:051302

Walton OR. 1994. Numerical simulation of inelastic frictional particle-particle interaction. In *Particulate Two-Phase Flows*, ed. MC Roco, pp. 884–911. Oxford, UK: Butterworth-Heinemann

Walton OR. 2008. Review of adhesion fundamentals for micron-scale particles. *KONA Powder Part. J.* 26:129–41

Walton OR, Johnson SM. 2009. Simulating the effects of interparticle cohesion in micron-scale powders. *AIP Conf. Proc.* 1145:897–900

Wang G, Yu W, Zhou C. 2006. Optimization of the rod chain model to simulate the motions of a long flexible fiber in simple shear flows. *Eur. J. Mech. B* 25:337–47

Weber MW, Hrenya CM. 2006. Square-well model for cohesion in fluidized beds. *Chem. Eng. Sci.* 61:4511–27

Wegner S, Börzsönyi T, Bien T, Rose G, Stannarius R. 2012. Alignment and dynamics of elongated cylinders under shear. *Soft Matter* 9:10950–58

Willett CD, Adams MJ, Johnson SA, Seville JPK. 2000. Capillary bridges between two spherical bodies. *Langmuir* 16:9396–405

Williams J, O'Connor R. 1999. Discrete element method and the contact problem. *Arch. Comput. Methods Eng.* 6:279–304

Wouterse A, Williams SR, Philipse AP. 2007. Effect of particle shape on the density and microstructure of random packings. *J. Phys. Condens. Matter* 19:406215

Wu J, Aidun CK. 2010. A method for direct simulation of flexible fiber suspensions using lattice Boltzmann equation with external boundary force. *Int. J. Multiphase Flow* 36:202–9

Yamamoto S, Matsuoka T. 1993. A method for dynamic simulation of rigid and flexible fibers in a flow field. *J. Chem. Phys.* 98:644–50

Yang J, Wu CY, Adams M. 2013a. DEM analysis of effects of particle properties and mixing conditions on particle attachment processes. *AIP Conf. Proc.* 1542:967–70

Yang M, Li S, Liu G, Yao Q. 2013b. Electrically-enhanced deposition of fine particles on a fiber: a numerical study using DEM. *AIP Conf. Proc.* 1542:943–46

Yang RY, Yu AB, Choi SK, Coates MS, Chan HK. 2008a. Agglomeration of fine particles subjected to centripetal compaction. *Powder Technol.* 184:122–29

Yang RY, Zou RP, Yu AB. 2003. Numerical study of the packing of wet coarse uniform spheres. *AIChE J.* 49:1656–66

Yang RY, Zou RP, Yu AB, Choi SK. 2008b. Characterization of interparticle forces in the packing of cohesive fine particles. *Phys. Rev. E* 78:031302

Yang S, Dong K, Zou RP, Yu AB. 2012. *DEM simulation of dust cake formation related to electrostatic precipitation*. Presented at Int. Symp. Chem. React. Eng., Maastricht, Neth., Sept. 2–5

Ye M, van der Hoef MA, Kuipers JAM. 2004. A numerical study of fluidization behavior of Geldart A particles using a discrete particle model. *Powder Technol.* 139:129–39

Zhang R, Li J. 2007. Simulation on mechanical behavior of cohesive soil by distinct element method. *J. Terramech.* 43:303–16

Zhu H, Zhou Z, Yang RY, Yu AB. 2007. Discrete particle simulation of particulate systems: theoretical developments. *Chem. Eng. Sci.* 62:3378–96

Zhu H, Zhou Z, Yang RY, Yu AB. 2008. Discrete particle simulation of particulate systems: a review of major applications and findings. *Chem. Eng. Sci.* 63:5728–70

Zhu R, Li S, Yao Q. 2013. Effects of cohesion on the flow patterns of granular materials in spouted beds. *Phys. Rev. E* 87:022206